ANL/RA/CP-98611

Space-Angle Approximations in the Variational Nodal Method

E. E. Lewis
Department of Mechanical Engineering
Northwestern University
Evanston, IL 60208 (U.S.A.)

and

G. Palmiotti and T. Taiwo
Reactor Analysis Division
9700 S. Cass Avenue
Argonne National Laboratory
Argonne, IL 60439 (U.S.A.)

To be presented at the M&C'99 Conference,
September 27-30, 1999
Madrid, Spain

This work was supported by the U.S. Department of Energy under contract No. W-31-109-ENG-38.

DISCLAIMER

Space-Angle Approximations in the Variational Nodal Method

E. E. Lewis
Department of Mechanical Engineering
Northwestern University
Evanston, IL 60208 (U.S.A.)
e-lewis@nwu.edu

G. Palmiotti and T. Taiwo
Reactor Analysis Division
Argonne National Laboratory
Argonne, IL 60439 (U.S.A.)
GPalmiotti@anl.gov; Taiwo@anl.gov

Abstract

The variational nodal method is formulated such that the angular and spatial approximations may be examined separately. Spherical harmonic, simplified spherical harmonic, and discrete ordinate approximations are coupled to the primal hybrid finite element treatment of the spatial variables. Within this framework, two classes of spatial trial functions are presented: (1) orthogonal polynomials for the treatment of homogeneous nodes and (2) bilinear finite subelement trial functions for the treatment of fuel assembly sized nodes in which fuel-pin cell cross sections are represented explicitly. Polynomial and subelement trial functions are applied to benchmark water-reactor problems containing MOX fuel using spherical harmonic and simplified spherical harmonic approximations. The resulting accuracy and computing costs are compared.

1. Introduction

The variational nodal method (VNM) is cast within the standard multigroup treatment of the energy variables. It is based on a primal hybrid finite element formulation of the even–parity form of the Boltzmann equation with odd-parity Lagrange multipliers coupling the subdomains which in the nuclear literature are referred to as nodes. Since first implemented in the VARIANT code (Carrico, 1995; Palmiotti, 1995; Lewis, 1996), the method has been generalized to allow additional classes of angular and spatial trial functions to be used combined to meet a wider variety of computational cost and physical modeling objectives. Thus, at present, simplified spherical harmonics (SPn) approximations can substituted for full spherical harmonics (Pn) expansions to achieve substantial cost savings often without a commensurate loss of accuracy (Lewis, 1997). Likewise, the orthogonal trial functions describing spatial distribution of the even-parity flux within a node may be replaced by an array of rectangular subelements with bilinear trial functions (Lewis, 1998). The subelement formulation, thus far implemented only in x-y geometry, eliminates the need to homogenize cross sections at the fuel assembly level or of performing fine-mesh calculations with one node per fuel pin cell. Pin powers to be extracted directly from full core VNM calculations utilizing one node per assembly, and for which homogenizing has been applied only at the fuel-pin cell level.

In what follows, we first review the variational basis for VNM. In section 3, we perform the Pn expansions to show that the reduced hybrid element formulations consists of coupled sets of second order equations and their Lagrange multipliers. The angular approximation is contained entirely within coupling matrices. Thus other angular approximations, even some that may not be deduced directly from the variational principle, can be incorporated simply by changing these matrices. This, in particular, allows the spatial variables of SPn and discrete ordinate (Sn) methods to be treated within the hybrid finite element framework of the variational nodal method. In section 4, we present a unified treatment of the discretization of the spatial variables, using both orthogonal polynomials and bilinear subelements to represent the spatial distribution within the node. In section 5, we present a series of calculations for MOX fuel assemblies in a light-water reactor core. With Pn and SPn approximations in angle, accuracy and computational cost comparisons are made between orthogonal polynomial and subelement trial functions is space.

2. Variational Principle

The variational nodal method is a primal hybrid finite element representation of the even-parity form of the transport equation. In the hybrid formulation, the problem domain V is decomposed into subdomains V_ν (also called elements or nodes):

$$V=\sum_\nu V_\nu. \tag{1}$$

Within each node, the even-parity form of the transport equation is solved in space ($\vec{r}$) and angle ($\hat{\Omega}$):

$$-\hat{\Omega}\cdot\vec{\nabla}\sigma^{-1}\hat{\Omega}\cdot\vec{\nabla}\psi^+(\vec{r},\hat{\Omega})+\sigma\,\psi^+(\vec{r},\hat{\Omega})=\sigma_s\int d\hat{\Omega}'\psi^+(\vec{r},\hat{\Omega}')+s(\vec{r}),\quad \vec{r}\in V_\nu \tag{2}$$

where ψ^+ is the even parity flux component, σ and σ_s the total and scattering cross sections and s the group source. The odd-parity flux ψ^-, which is related to ψ^+ by

$$\hat{\Omega}\cdot\vec{\nabla}\psi^+(\vec{r},\hat{\Omega})+\sigma\psi^-(\vec{r},\hat{\Omega})=0,\qquad \vec{r}\in\Gamma_\nu \tag{3}$$

is defined only along the node interfaces as a Lagrange multiplier.

The functional for the variational nodal method is given as a superpositon of nodal contributions

$$F[\psi^+,\psi^-]=\sum_\nu F_\nu[\psi^+,\psi^-], \tag{4}$$

where

$$F_\nu[\psi^+,\psi^-]=\int_\nu dV\left\{\int d\hat{\Omega}[\sigma^{-1}(\hat{\Omega}\cdot\vec{\nabla}\psi^+)^2+\sigma\psi^{+2}]-\sigma_s\phi^2-2\phi s\right\}+2\int_\nu d\Gamma\int d\hat{\Omega}\hat{\Omega}\cdot\hat{n}\psi^+\psi^-. \tag{5}$$

This functional must be stationary with respect to arbitrary variations $\tilde{\psi}^+$ and $\tilde{\psi}^-$ about the true solutions ψ^+ and ψ^-. Thus, we make the replacements $\psi^+\to\psi^++\delta\tilde{\psi}^+$ and $\psi^-\to\psi^-+\varepsilon\tilde{\psi}^-$ where δ and ε are small positive constants, and require the linear terms in δ and ε to vanish. Setting the linear term in δ to zero yields the weak form of Eq.(2)

$$\int_\nu dV\int d\hat{\Omega}[\sigma^{-1}(\hat{\Omega}\cdot\vec{\nabla}\tilde{\psi}^+)(\hat{\Omega}\cdot\vec{\nabla}\psi^+)+\tilde{\psi}^+(\sigma\psi^+-\sigma_s\phi-s)]+\int_\nu d\Gamma\int d\hat{\Omega}\hat{\Omega}\cdot\hat{n}\tilde{\psi}^+\psi^-=0, \tag{6}$$

and applying the divergence theorem yields

$$\int_V dV \int d\Omega \tilde{\psi}^+ (-\hat{\Omega}\cdot\bar{\nabla}\sigma^{-1}\hat{\Omega}\cdot\bar{\nabla}\psi^+ + \sigma\psi^+ - \sigma_s\phi - s) + \int_V d\Gamma \int d\Omega \hat{\Omega}\cdot\hat{n}\tilde{\psi}^+(\psi^- + \sigma^{-1}\hat{\Omega}\cdot\bar{\nabla}\psi^+) = 0. \tag{7}$$

Clearly, Eq. (2) must be satisfied if the volume integral is to vanish for arbitrary $\tilde{\psi}^+$, and Eq. (3) must be met at the interface for the surface integral to vanish. The continuity conditions across nodal interfaces may be stated as follows. Since the Lagrange multiplier ψ^- and its variation $\tilde{\psi}^-$ are uniquely defined at the interface, two conditions are imposed. First, the surface integral in Eq. (7) imposes continuity on $\sigma^{-1}\hat{\Omega}\cdot\bar{\nabla}\psi^+$. Second, requiring the linear term in ε to vanish yields for each nodal interface, say between nodes V_ν and $V_{\nu'}$, a condition of the form

$$\int_\nu d\Gamma \int d\Omega \hat{\Omega}\cdot\hat{n}\tilde{\psi}^-(\psi^+ - \psi'^+) = 0, \tag{8}$$

since $\hat{n}_\nu = -\hat{n}_{\nu'}$. Thus ψ^+ must be continuous across the interface.

3. Angular Approximations

To discretize the angular variable, we write the M and N terms in the even- and odd-order spherical harmonics as the vectors $\mathbf{g}(\hat{\Omega})$ and $\mathbf{k}(\hat{\Omega})$, respectively. These then obey the orthonormal conditions $\int d\Omega \mathbf{g}(\hat{\Omega})\mathbf{g}^T(\hat{\Omega}) = \mathbf{I}_M$, $\int d\Omega \mathbf{k}(\hat{\Omega})\mathbf{k}^T(\hat{\Omega}) = \mathbf{I}_N$ and $\int d\Omega \mathbf{g}(\hat{\Omega})\mathbf{k}^T(\hat{\Omega}) = \mathbf{0}$
The spherical harmonics approximations is then

$$\psi^+(\bar{r},\hat{\Omega}) = \mathbf{g}^T(\hat{\Omega})\psi^+(\bar{r}) \qquad \bar{r}\in V_\nu \tag{9}$$

and

$$\psi^-(\bar{r},\hat{\Omega}) = \mathbf{k}^T(\hat{\Omega})\psi^-(\bar{r}), \qquad \bar{r}\in \Gamma_\nu \tag{10}$$

where $\psi^+(\bar{r})$ and $\psi^-(\bar{r})$ are vectors of the spatially dependent coefficients of the even- and odd-parity spherical harmonics. Inserting these approximations into Eqs.(4) and (5) yields the reduced functional

$$F[\psi^+,\psi^-] = \sum_\nu F_\nu[\psi^+,\psi^-] \tag{11}$$

with

$$F_\nu[\psi^+,\psi^-] = \int_V dV \left\{\sigma^{-1}(\bar{\nabla}\cdot\bar{\mathbf{E}}^T\psi^+)^T(\bar{\nabla}\cdot\bar{\mathbf{E}}^T\psi^+) + \psi^{+T}(\sigma\mathbf{I} - \sigma_s\mathbf{w}\mathbf{w}^T)\psi^+ - 2\psi^{+T}\mathbf{s}\right\} + 2\int_V d\Gamma \psi^{+T}\hat{n}\cdot\bar{\mathbf{E}}\psi^- \tag{12}$$

and $[\mathbf{w}]_m = \delta_{m1}$, $\bar{\mathbf{E}} = \int d\Omega \hat{\Omega}\mathbf{g}(\hat{\Omega})\mathbf{k}^T(\hat{\Omega})$, $\mathbf{s} = \int d\Omega \mathbf{g}(\hat{\Omega})s(\bar{r})$.

We require this functional to be stationary by making the substitutions $\psi^+ \to \psi^+ + \delta\tilde{\psi}^+$ and $\psi^- \to \psi^- + \varepsilon\tilde{\psi}^-$ in Eqs. (11) and (12), where $\tilde{\psi}^\pm$ are variations about the true solutions $\psi^\pm$. We require the linear terms in δ and ε to vanish. Parallel to the exact case we obtain the Euler-Lagrange equations within the node to be

$$-\vec{\nabla}\cdot\sigma^{-1}\vec{\mathbf{E}}\vec{\mathbf{E}}^T\cdot\vec{\nabla}\psi^+(\vec{r})+\sigma\psi^+(\vec{r})=\sigma_s\mathbf{w}\mathbf{w}^T\psi^+(\vec{r})+\mathbf{s}(\vec{r}),\qquad \vec{r}\in V_\nu \tag{13}$$

with

$$\psi^-(\vec{r})=-\sigma^{-1}\vec{\nabla}\cdot\vec{\mathbf{E}}^T\psi^+(\vec{r}),\qquad \vec{r}\in\Gamma_\nu \tag{14}$$

where the orthonomal properties of $\mathbf{g}(\hat{\Omega})$ may be used to show that

$$\vec{\mathbf{E}}\vec{\mathbf{E}}^T=\int d\hat{\Omega}\hat{\Omega}\mathbf{g}(\hat{\Omega})\mathbf{g}^T(\hat{\Omega})\hat{\Omega}. \tag{15}$$

Continuity conditions on $\psi^\pm$ across nodal interfaces are met because ψ^- and $\tilde{\psi}^-$ are uniquely defined at the interface. The requirement that the linear term in ε vanish thus leads to the condition between neighboring nodes V_ν and $V_{\nu'}$:

$$\int_{\nu\gamma} d\Gamma\tilde{\psi}^-\hat{n}_\gamma\cdot\vec{\mathbf{E}}(\psi^+-\psi'^{+'})=0, \tag{16}$$

where ψ^+ and ψ'^+ are on opposite sides of the interface, showing that $\psi^+(\vec{r})$ is continuous across $\vec{r}\in\Gamma_\nu$.

Careful examination of Eqs. (13) and (14) indicates that by varying the forms of the coupling matrices $\vec{\mathbf{E}}$ other approximations may be written in terms of the variational principle. In particular, we let $\mathbf{g}(\mu)$ and $\mathbf{k}(\mu)$ be vectors of the M and N components of the orthonormal Legendre polynomials. Then we define

$$\mathbf{E}_o=\tfrac{1}{2}\int_{-1}^{1}d\mu\mu\mathbf{g}(\mu)\mathbf{k}^T(\mu). \tag{17}$$

If we then take the components of the vector matrix $\vec{\mathbf{E}}$ as $\mathbf{E}_k=[\delta_{k1},\delta_{k2},\delta_{k3}]\otimes\mathbf{E}_o$, where $\otimes$ indicates Kronecker tensor multiplication, then the foregoing equations reduce to the simplified spherical harmonics approximation. Moreover, analogous to Eq. (15) we may show that

$$\mathbf{E}_o\mathbf{E}_o^T=\tfrac{1}{2}\int_{-1}^{1}d\mu\mu^2\mathbf{g}(\mu)\mathbf{g}^T(\mu). \tag{18}$$

Finally, if we view Eqs. (11) and (12) simply as the variational principle for a coupled set of partial differential equations in space, we combine discrete ordinate collocation with the hybrid finite element approach by defining,

$$[\psi^\pm(\vec{r})]_m=\sqrt{\omega_m}\psi^\pm(\vec{r},\hat{\Omega}_m), \tag{19}$$

where $\hat{\Omega}_m$ and ω_m refer to the discrete directions and weights, and letting $[\mathbf{E}_k]_{mn}=\hat{\Omega}_m\cdot\hat{n}_k\delta_{mn}$, $[\mathbf{w}]_m=\sqrt{\omega_m}$ and $[\mathbf{s}(\vec{r})]_m=\sqrt{\omega_m}s(\vec{r})$. Thus, the reduced functional, Eq. (12) may serve as a basis for applying primal hybrid finite element methods to Pn, SPn, and Sn approximations.

4. Spatial Discretization

Two different classes of trial functions are used currently to describe the spatial distribution of the even-parity flux within the node. We first review the orthogonal polynomials used in earlier work, and then present a new finite subelement formulation. In both cases, orthogonal polynomials are used to represent the odd-parity distributions at the node interfaces.

To examine the orthogonal polynomial trial functions, we begin by using the Kronecker tensor product to expand the even-parity flux coefficients within the node as

$$\psi^+(\vec{r}) = \mathbf{I}_M \otimes \mathbf{f}^T(\vec{r})\xi_\nu , \qquad \vec{r} \in V_\nu \tag{20}$$

where the I spatial trial functions obey the orthogonality condition

$$\int_\nu dV \mathbf{f}\mathbf{f}^T = V_\nu \mathbf{I}_I . \tag{21}$$

Along the node interface, we make the expansion

$$\psi^-(\vec{r}) = \mathbf{I}_N \otimes \mathbf{h}^T(\vec{r})\chi_\nu, \qquad \vec{r} \in \Gamma_\nu \tag{22}$$

where the J spatial trial functions obey the orthogonality condition

$$\int_\nu d\Gamma \mathbf{h}\mathbf{h}^T = \mathbf{I}_J . \tag{23}$$

Inserting these approximations into Eqs. (11) and (12) reduces the functional to algebraic form

$$F = \sum_\nu F_\nu[\zeta_\nu, \chi_\nu] \tag{24}$$

and

$$F_\nu[\zeta_\nu, \chi_\nu] = \zeta_\nu^T \mathbf{A}_\nu \zeta_\nu - 2\zeta_\nu^T \mathbf{s}_\nu + 2\zeta_\nu^T \mathbf{M}_\nu \chi_\nu . \tag{25}$$

Here,

$$\mathbf{A}_\nu = \sigma_\nu^{-1} \mathbf{E}_k \mathbf{E}_{k'}{}^T \otimes \int_\nu dV (\nabla_k \mathbf{f})(\nabla_{k'} \mathbf{f}^T) + (\sigma_\nu \mathbf{I}_M - \sigma_{s\nu} \mathbf{w}\mathbf{w}^T) \otimes V_\nu \mathbf{I}_I , \tag{26}$$

where repeated subscripts k or k' indicates summation, and

$$\mathbf{M}_\nu = \mathbf{E}_k \otimes \int_\nu d\Gamma n_k \mathbf{f}\mathbf{h}^T \tag{27}$$

with the source

$$\mathbf{s}_\nu = \int_\nu dV \mathbf{s} \otimes \mathbf{f} . \tag{28}$$

With orthogonal trial functions, we have assumed that the cross sections are uniform over the entire node. If they are not, it is difficult to accurately represent the spatial distribution of the flux using smooth polynomial (Fanning, 1997); an alternative is to employ fine-grid nodes in a two-level iteration scheme (Ruggieri, 1996). We approached the problem by subdividing the node V_ν into a number of subelements.

$$V_\nu = \sum_e V_e . \tag{29}$$

In particular, we divide square nodes into an array of square subelements. Within each subelement, we represent the spatial distribution by four bilinear trial functions, designated by the vector $\mathbf{n}(\vec{r})$, and a *vector of unknown magnitudes* ξ_e. The even-parity flux moments become

$$\psi^+(\vec{r}) = \mathbf{I}_M \otimes \mathbf{n}^T(\vec{r})\xi_e . \qquad \vec{r} \in V_e \tag{30}$$

If we retain Eq. (22) to represent the interface term, the nodal functional given by Eq. (12) reduce to a superposition of subelement contributions:

$$F_\nu[\zeta_\nu, \chi_\nu] = \sum_e \xi_e^T \mathbf{A}_e \xi_e - 2\sum_e \xi_e^T \mathbf{s}_e + 2\sum_e \xi_e^T \mathbf{M}_e \chi_\nu , \tag{31}$$

where the coefficient matrices are again given in terms of the known trial functions

$$\mathbf{A}_e = \sigma_e^{-1}\mathbf{E}_k\mathbf{E}_{k'}{}^T \otimes \int_e dV(\nabla_k \mathbf{n})(\nabla_{k'}\mathbf{n}^T) + (\sigma_e \mathbf{I} - \sigma_{se}\mathbf{w}\mathbf{w}^T) \otimes \int_e dV \mathbf{n}\mathbf{n}^T , \tag{32}$$

and

$$\mathbf{M}_e = \mathbf{E}_k \otimes \int_e d\Gamma n_k \mathbf{n}\mathbf{h}^T , \tag{33}$$

with source term

$$\mathbf{s}_e = \int_e dV \mathbf{s} \otimes \mathbf{n} . \tag{34}$$

With piecewise bilinear trial functions for the subelements, the components of ξ_e are just the approximate values of ψ^+ at the subelement vertices. Since these trial functions must be continuous across subelement interfaces, the components of ξ_e corresponding to the same physical location on either side of a subelement must have the same value. This continuity condition is enforced by creating a Boolean matrix Ξ_ε for each subelement that maps the ξ_e onto ζ_ν, a node wide vector of coefficients:

$$\xi_e = \Xi_\varepsilon \zeta_\nu . \tag{35}$$

This transformation allows us to write the discretized functional in the form of Eq. (25). Now, however, the known matrices and source terms are each a superposition of subelemental contributions: $\mathbf{A}_\nu = \sum_e \Xi_\varepsilon^T \mathbf{A}_e \Xi_\varepsilon$, $\mathbf{M}_\nu = \sum_e \Xi_\varepsilon^T \mathbf{M}_e$ and $\mathbf{s}_\nu = \sum_e \Xi_\varepsilon^T \mathbf{s}_e$.

We may now obtain a set of algebraic equations by requiring the discretized functional to be stationary. To examine arbitrary variations about the true solutions, we make the replacements $\zeta_\nu \to \zeta_\nu + \delta\tilde{\zeta}_\nu$ and $\chi_\nu \to \chi_\nu + \delta\tilde{\chi}_\nu$ in Eqs. (24) and (25). Requiring the linear term in δ to vanish yields

$$\mathbf{A}_\nu \zeta_\nu + \mathbf{M}_\nu \chi_\nu = \mathbf{s}_\nu . \tag{36}$$

Requiring the linear term in ε to vanish imposes continuity across nodal interfaces of the moments defined by

$$\psi_\nu = \mathbf{M}_\nu^T \zeta_\nu . \tag{37}$$

We may solve Eq. (36) for ζ_ν,

$$\zeta_\nu = \mathbf{A}_\nu^{-1}\mathbf{s}_\nu - \mathbf{A}_\nu^{-1}\mathbf{M}_\nu \chi_\nu \tag{38}$$

and combine with Eq. (37) to obtain

$$\psi_\nu = \mathbf{M}_\nu^T \mathbf{A}_\nu^{-1}\mathbf{s}_\nu - \mathbf{M}_\nu^T \mathbf{A}_\nu^{-1}\mathbf{M}_\nu \chi_\nu . \tag{39}$$

At this point, we have written the even-parity flux moments ψ_ν at the node interface in terms of the source and the odd-parity interface moments χ_ν, while imposing the continuity of both of these moments between neighboring elements. The final step is to transform variables such that Eq. (39) may be written in terms of a response matrix. Introducing the partial current like variables

$$\mathbf{j}_\nu^{\pm} = \tfrac{1}{4}\psi_\nu \pm \tfrac{1}{2}\chi_\nu \tag{40}$$

into Eq. (39) and (40) then yields response matrix equation for each node:

$$\mathbf{j}_\nu^{+} = \mathbf{R}_\nu \mathbf{j}_\nu^{-} + \mathbf{B}_\nu \mathbf{s}_\nu , \tag{41}$$

where $\mathbf{R}_\nu = \left(\tfrac{1}{2}\mathbf{M}_\nu^T \mathbf{A}_\nu^{-1}\mathbf{M}_\nu + \mathbf{I}\right)^{-1}\left(\tfrac{1}{2}\mathbf{M}_\nu^T \mathbf{A}_\nu^{-1}\mathbf{M}_\nu - \mathbf{I}\right)$ and $\mathbf{B}_\nu = \left(\tfrac{1}{2}\mathbf{M}_\nu^T \mathbf{A}_\nu^{-1}\mathbf{M}_\nu + \mathbf{I}\right)^{-1}\tfrac{1}{2}\mathbf{M}_\nu^T \mathbf{A}_\nu^{-1}$.

5. Results

Comparisons of polynomial and subelement trial functions and of Pn and SPn angular approximations have been performed for configurations consisting of the pressurized water reactor (PWR), MOX, and UO_2 assemblies. Two-group cross sections and detailed geometric descriptions are published elsewhere (Cavarec, 1994). For each of the problems considered two spatial approximations are compared. In the first, each assembly constitutes one node with quadratic interface conditions. Each node, however, is not homogenized but contains an internal 17x17 array of bilinear subelements, each representing the unique cross sections for one homogenized fuel-pin cell with a uniform group source. In the second, reference fine-grid method, each fuel pin cell is represented by one homogeneous node with the internal flux distribution expanded as a fourth order polynomial, and the interface conditions taken to be quadratic polynomials.

The first configuration considered is the quarter-core benchmark problem, designated as case C5 (Cavarec, 1994). With quarter-core symmetry, the problem contains only two MOX and two UO_2 assemblies, surrounded by a reflector. Nevertheless, steep global flux gradients across the assemblies provide a computational challenge. Results are tabulated in Table 1. Good agreement between eigenvalues, maximum and average pin powers is indicated. The effects of increasing the angular approximation to P5 or of going to cubic interface conditions were found to be small and therefore, are not included in the tables. The P1, SP3, and P3 approximations with quadratic interface conditions are employed for larger problems.

We have applied the fine-grid and subelement methods to rodded and unrodded full-core reflected configurations consisting of 157 fueled assemblies. The rodded layout is shown in Fig. 1; unrodded

replace rodded UO_2 assemblies in the unrodded configuration. The rodded configuration in particular, presents quite severe power distributions, and Table 2 and Figs. 2 through 4 indicate that it is the most error prone. Figures 2 and 3 indicate that the largest pin power errors occur not in the high power density MOX assemblies, but rather adjacent to inserted control rods in the UO_2 assemblies. Figure 4 also shows the largest assembly power differences to be in the rodded UO_2 assemblies.

The errors introduced by the quadratic approximations between assemblies appear to be small. We have refined the interface LaGrange multipliers to cubic and quartic polynomials, and no significant changes result. More likely, the errors for the rodded case may be reduced substantially by replacing bilinear with quadratic subelement trial functions in the rodded assemblies.

Table 3 compares the computational effort required for the full-core problems using P3 approximations subelement and fine-grid approaches. The subelement method shifts computational effort from the solution of the response matrix equations during the outer iterations to the formation of the response matrices. With subelements, the detailed power distribution within the assemblies is determined before the outer iterations are initiated, while the relatively few assembly-sized nodes cause the response matrix solution algorithm to run faster and converge in fewer iterations. The response matrix formation CPU time increases linearly with the number of unique fuel assembly types, but these calculations are totally independent of one another, offering a strong computational advantage if calculations were to be performed on parallel machines.

6. Conclusions

Within the framework of the variational nodal method, polynomial and finite subelement approaches used in combination with Pn or SPn angular approximations provide substantial flexibility in cost-accuracy tradeoffs for doing whole-core transport calculations. The subelement method, in particular, offers an alternative to the conventional strategy of performing infinite lattice calculations to obtain homogenized assembly cross sections before global diffusion or transport calculations are undertaken. Moreover, the subelement approach reduces CPU times from those required for full-core fine-grid transport calculations. For rodded assemblies, further accuracy may be pursued through refinement of the subelement trial functions. Extensions to include axial power distributions (i.e., three-dimensional calculations) within the subelement formulation appear to be feasible.

Acknowledgements

This work was supported by the U.S. Department of Energy under Contract No. W-31-109-ENG-38 and by U.S. Department of Energy Contract No. DE-FG07-98ID13632.

References

[Cavarec, 1994] Cavarec, C., et al., "The OECD/NEA Benchmark Calculations of Power Distributions within Assemblies," Electricite de France, Sept. 1994

[Carrico, 1995] Carrico, C. B., Palmiotti, G., Lewis, E. E., "Progress and Applications of the Variational Nodal Method," Proc. Int. Topl. Mtg. on Mathematics and Computation, Portland, OR, April, 1995

[Fanning, 1997] Fanning, T. H., Palmiotti, G., "Variational Nodal Transpoert with Heterogeneous Nodes," Nucl. Sci. Eng. **127**, 154 (1997)

[Lewis, 1996], Lewis, E. E., C. B. Carrico, Palmiotti, G., "Variational Nodal Formulation of the Spherical Harmonics Equations," Nucl. Sci. Eng. **122**, 194, 1996

[Lewis, 1997], Lewis, E. E., Palmiotti, G., "Simplified Spherical Harmonics in the Variational Nodal Method," Nucl. Sci. Eng., **126**, 48, 1997

[Lewis, 1998], Lewis, E. E., Palmiotti, G., "A Finite Subelement Formulation of the Variational Nodal Method," Trans. Am. Nucl. Soc. **79**, 144 (1998)

[Palmiotti, 1995] Palmiotti, G., Lewis, E. E., Carico, C. B., "VARIANT: VARIational Anisotropic Nodal Transport for Multidimensional Cartesian and Hexagonal Geometry Calculation," Argonne National Laboratory ANL-95/40, 1995

[Ruggieri] Ruggieri, J. M., Boyer, R., Doriath, J. Y., Finck, P. J., "Accounting for Strong Localized Heterogeneities and Local Transport Effect in Core Calculation," Nucl. Sci. Engr. **124**, 82 (1996)

Table 1. Subelement/Fine-Grid Comparisons
for Benchmark Case C5

Approximation:	P1	SP3	P3
% Difference : k-eff	0.01	0.07	0.07
% Difference: Max. pin fission rate	0.48	-0.07	0.12
% Ave. absolute difference: pin fission rate	1.20	0.78	0.75

Table 2. Subelement/Fine-Grid Comparisons for Whole-Core Case

	Unrodded Core			Rodded Core		
Approximation:	P1	SP3	P3	P1	SP3	P3
% Difference: k-eff	0.12	0.08	0.08	-0.34	-0.19	-.021
% Difference: Max pin fission rate	2.92	1.86	2.17	0.19	0.38	0.55
% Ave. absolute difference: pin fission rate	0.81	0.51	0.51	4.10	2.86	3.06

Table 3. CPU Times for Subelement and Fine-Grid
Whole-Core Calculations (P3 Rodded Core)

	Subelement	Fine-Grid
R-Matrix Formation, s	73.5	0.2
Outer Iterations, s	38.3	910.0
Total, s	111.8	910.2

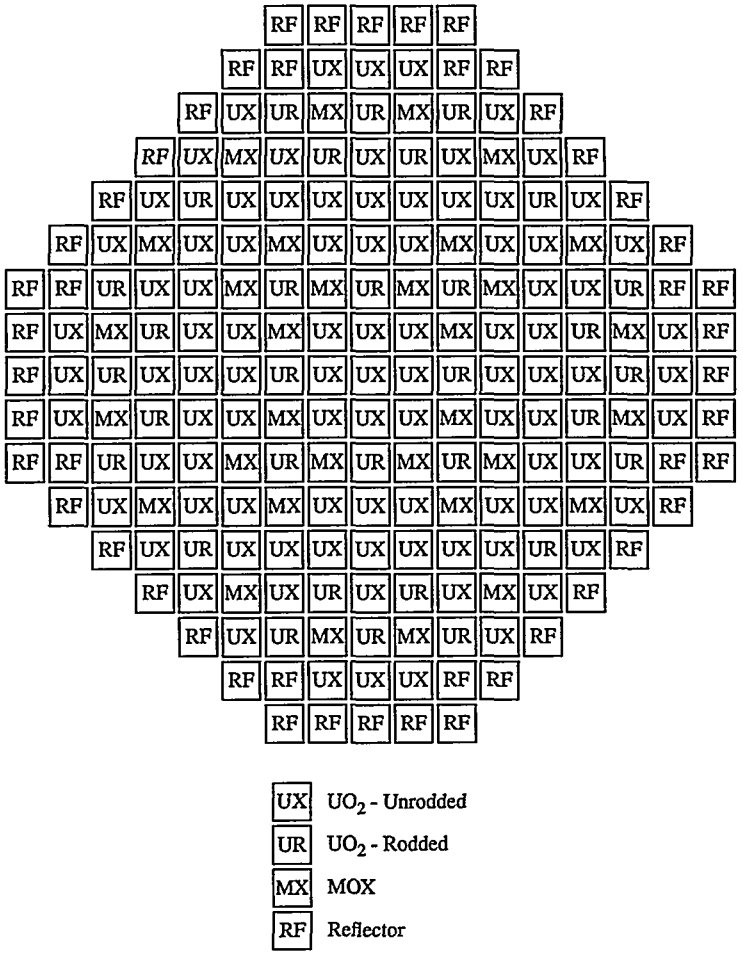

Fig. 1. Layout for the MOX/UO_2 PWR Problem.

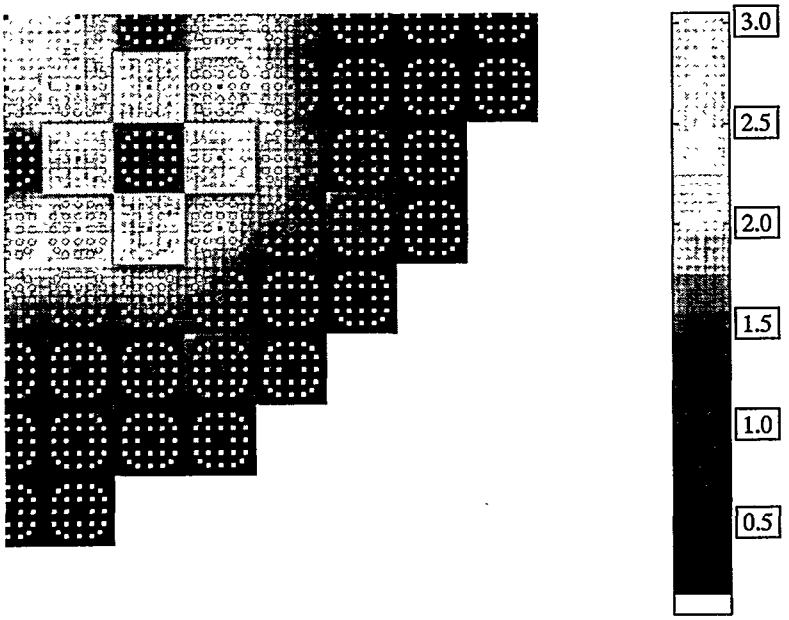

Fig. 2. Radial Pin Power Distribution for the Southeast Quadrant for the Rodded Case.

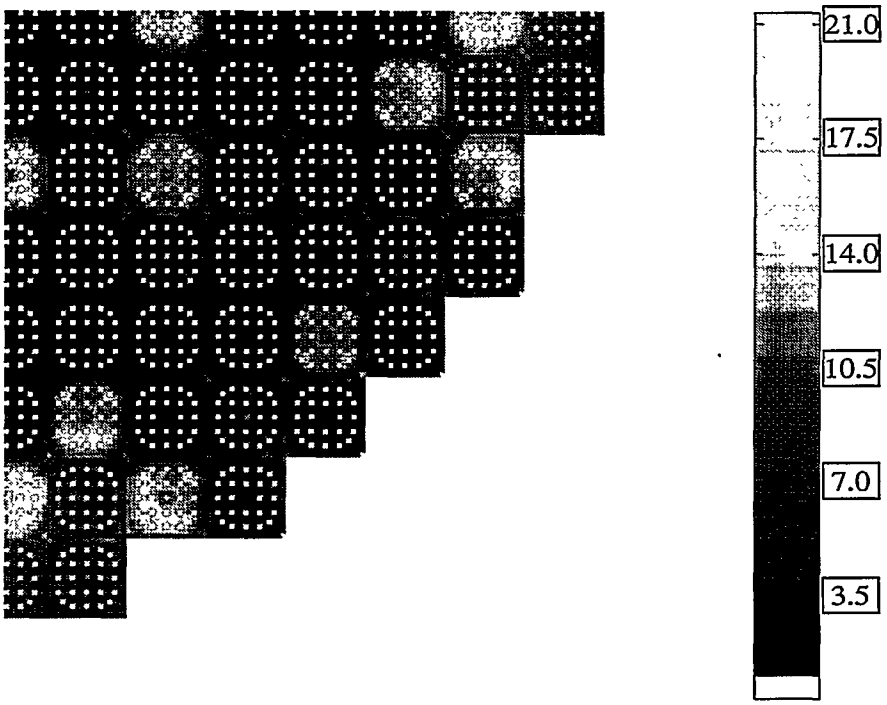

Fig. 3. Differences (%) between Subelement and Fine-Grid Calculated Pin Powers for the Rodded Case.

-0.3 0.2	-0.3 -0.7	-0.3 -7.2	-0.2 0.1	-0.2 1.1	-0.1 -1.5	-0.1 -10.4	0.2 -6.4
-0.3 -0.7	-0.3 -0.8	0.3 -1.0	-0.2 0.6	-0.1 1.3	-0.1 -6.1	0.5 -4.7	0.3 -5.2
-0.3 -7.2	0.3 -1.0	-0.3 -6.7	0.4 1.6	-0.1 2.2	-0.1 1.1	0.1 -6.5	
-0.2 0.1	-0.2 0.6	0.4 1.6	-0.1 2.0	-0.1 2.2	0.5 2.9	0.3 1.8	
-0.2 1.1	-0.1 1.3	-0.1 2.2	-0.1 2.2	0.0 2.9	0.3 1.5		
-0.1 -1.5	-0.1 -6.1	-0.1 1.1	0.5 2.9	0.3 1.5			
0.1 -10.4	0.5 -4.7	0.1 -6.5	0.3 1.8				
0.2 -6.4	0.3 -5.2	Unrodded Rodded					

Fig. 4. Differences (%) between Subelement and Fine-Grid Calculated Assembly Powers for Unrodded and Rodded Configurations.